Journal of Sound and Vibration (2000) **238**(2), 309–325
doi:10.1006/jsvi.2000.3209, available online at http://www.idealibrary.com on IDEAL®

PREDICTION OF AEROELASTIC FLUTTER IN A HARD DISK DRIVE

B. C. KIM†

Dynamic Stability Laboratory, 1113 *Etcheverry Hall*, *University of California*, *Berkeley*, *CA*94720, *U.S.A.*

A. RAMAN

School of Mechanical Engineering, *Purdue University*, *West Lafayette*, *IN* 47907-1288, *U.S.A.*
E-mail: *raman@ecn.purdue.edu*

AND

C. D. MOTE, JR.

Glenn L. Martin Institute, *Professor of Engineering and President*, *University of Maryland*, *College Park*, *MD*20742, *U.S.A.*

(*Received* 2 *September* 1999, *and in final form* 21 *June* 2000)

An experimental technique to predict the onset of aeroelastic flutter of an enclosed computer memory disk is presented. The aerodynamic pressure is modelled as the sum of dissipative and circulatory linear operators, which subsumes as a special case the pressure generated in a thin hydrodynamic film between the disk and the wall. It is shown that the aeroelastic model parameters can be extracted from the frequency response function of the disk spinning at subcritical speeds. The aeroelastic parameters for an acoustically excited single disk at different enclosure gaps are derived for the speed range 6,000–19,800 rpm. The flutter speed predicted is strongly influenced by the enclosure gap and the substrate damping. A flutter speed as low as 35,000 rpm has been predicted. The technique can also be extended to predict the flutter speed in other systems including DVD and CDROM drives.

1. INTRODUCTION

The new generation of hard disk drives is expected to pack high track densities (20,000 + TPI) and rotate at very high speeds (20,000 + rpm). At rotation speed near and beyond 20,000 rpm the aeroelastic coupling between the disk vibration and the air around the disk is expected to be significant. This coupling leads to disk flutter, which can contribute significantly to the track misregistration and disk drive failure. Thus, the prediction of the aeroelastic flutter speed is crucial for the design of the new generation of disk drives.

The stability of the equilibrium configuration of floppy disks coupled through thin gas films to a rigid enclosure has been studied by a number of researchers [1–5]. While Chonan *et al.* [1] modelled the film as a linear elastic foundation, Hosaka and Crandall [2] and Renshaw [5] utilized thin film lubrication equations neglecting the effect of radial flow.

†Currently at Daewoo Electronics Co., Ltd. 60-8 Gasan Dong, Geumcheon Gu, Seoul 153-023, South Korea.

0022-460X/00/470309 + 17 $35.00/0

Huang and Mote [4] included the effect of radial flow and concluded that non-symmetric stiffening caused by the radial flow can cause combination instabilities in addition to the aeroelastic flutter. These have hitherto been mainly theoretical and numerical studies only.

The onset of aeroelastic flutter in disks spinning without enclosure (unbounded domains) has also been studied both analytically and experimentally. These include the works of D'Angelo and Mote [6], D'Angelo *et al.* [7] and Yasuda and Torii [8]. D'Angelo and Mote [6] and D'Angelo *et al.* [7] indicated that inviscid, compressible and incompressible potential flow models significantly overestimate the onset of the aeroelastic flutter speed. Yasuda and Torii [8] used an experiment-based flow–structure interaction model where the model parameters were calculated from the experimental knowledge of the flutter speed only. The present work can be considered as a generalization of Yasuda and Torii's work and includes a careful measurement of the speed dependence of the model parameters at pre-flutter speed.

The aeroelastic coupling problems in a hard disk are distinct from those of a disk in an unbounded enclosure or in a floppy disk for the following reasons.

(1) The flow boundary conditions in the disk drives are bounded radially and axially. The acoustic wavelengths are larger than the characteristic gap widths and this can cause a significant difference between flutter speed of the enclosed disk and the open disk.
(2) The rotation speeds in hard disk drives are greater than in floppy disks, and the gap widths are greater. This leads to a substantially greater flow Reynolds number and the use of hydrodynamic lubrication theory can lead to an inaccurate model of the aerodynamic pressure. The Reynolds number, for a commercially available 3·5 in. hard disk rotating at 10,000 rpm (Ω is the disk speed, R_2 is the outer disk radius, d is the gap spacing between the disk and the wall) is substantially greater than 1 ($R_e = \Omega R_2 d/v = 633 \gg 1$). Note that the Reynolds number of the flow between two corotating disks in a disk stack will be greater than this value because the inter-disk spacing is usually greater than the spacing between disk and the wall.
(3) The hard disks have high bending stiffness and for the satisfactory operations the disk must maintain a near flat equilibrium.
(4) The aluminum substrate in the disk has significant material damping, which must be modelled.
(5) The multiple disk stacks are normal and the outer disks in a stack are subject to a dissimilar flow conditions on their faces. A shear flow between the disk and rigid enclosure exists on one surface and flow in a corotating enclosure is present on the other side raising the question whether the outer disks are more susceptible to flutter than the inner ones.

This paper presents an experimental estimation technique for the flutter speed of a hard disk based on the measurements taken at subcritical speed. The technique is based on a simple fluid pressure model represented by a distributed, viscous pressure that rotates with respect to the disk, in a manner analogous to Hansen *et al.* [9]. This model approaches the special case of the pressure generated in a narrow gap at low Reynolds number. It is shown analytically that this form of aerodynamic loading differentially damps the forward and backward travelling waves. To illustrate this point, the frequency response function of an acoustically excited disk spinning at 19,800 rpm is shown in Figure 1. The excitation is sufficiently broadband to excite the modes of interest. The peaks representing travelling wave frequencies and the modes are labelled as shown. It is seen that the forward travelling waves are significantly more damped than the backward travelling waves. For instance, the forward travelling wave peak magnitude for the (0, 2) mode is nearly 17 dB lower than the backward travelling wave peak magnitude. The 3 dB bandwidth for the forward travelling

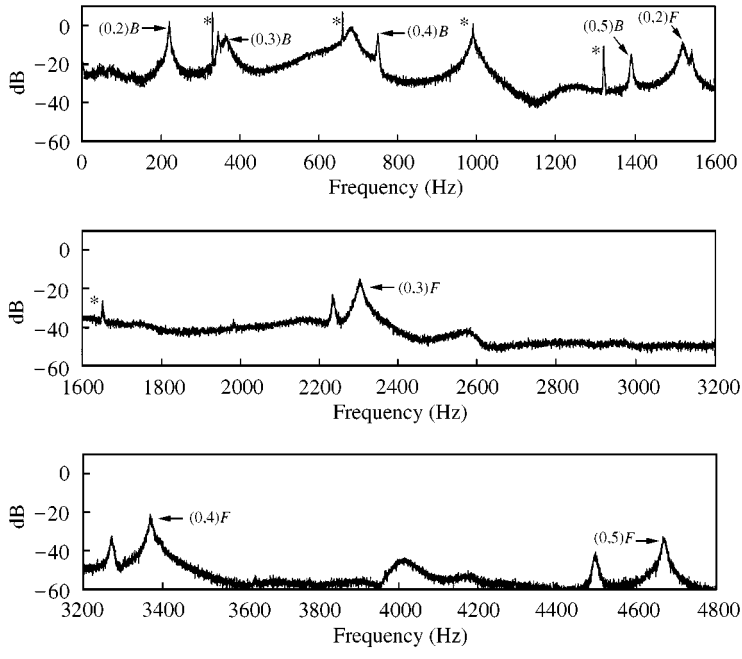

Figure 1. Magnitude of the frequency response function of an aerodynamically excited disk (disk speed: 19,800 rpm; *, runout frequencies). (m, n) refers to number of nodal circles and diameters, respectively, of the travelling wave. B and F represent the backward and forward travelling waves.

wave (≈ 10 Hz) is much greater than for the backward travelling wave (≈ 4 Hz). This differential damping is primarily due to airflow effects because in vacuum the damping of the forward and backward travelling waves is identical (Hansen *et al.* [9]). At higher-speeds damping of the backward travelling waves can vanish entirely leading to a travelling wave flutter instability. This result is exploited to extract model parameters from the frequency response function (FRF) of the acoustically excited disk at subcritical speeds. The method of Hansen *et al.* [9] is used to predict the supercritical speed at which the damping of a backward travelling wave vanishes and aeroelastic flutter occurs.

The results show that the flutter speed and mode are strongly dependent on the enclosure gap width. The flutter speed can be as low as 35,000 rpm. A strong dependence of the flutter speed on the gap width confirms that the onset of flutter can be affected through airflow control through the enclosure design. The results also indicate that the onset of the aeroelastic flutter should not be a concern for the impending generation of 20 000 rpm drives, but possibly for the next generation of 30,000 + rpm drives. Lastly, the technique used here can be applied to predict the flutter speed of optical disk systems used in the CDROM and DVD drives. Because the bending stiffness and natural frequencies are much smaller in these polycarbonate substrate disks, their flutter speed will also be lower. We note that CDROM drives have recently been shown to operate at supercritical speed [10] and thus operate much closer to their aeroelastic flutter speed.

2. THEORETICAL BACKGROUND

The theoretical development here is based on the work of Hansen *et al.* [9]. Consider a single annular disk of thickness h, clamping radius α, and outer radius b. Each disk in

a stack can be modelled as isolated if the effects of spindle flexibility and bearing clearance are neglected. The disk substrate is assumed to be isotropic, with Young's modulus E, Poisson's ratio ν, and density ρ. The disk spins at a constant speed Ω^*. A ground-fixed cylindrical co-ordinate frame (r^*, φ, z^*) is introduced. The acoustic waves from a speaker, over a small circular area centered about the point (r_f^*, φ_f), are used to excite the disk transversely. The aerodynamic pressure difference across the two faces of the disk is Δp^*. Because of the large bending stiffness the disk remains flat at equilibrium in the presence of aerodynamic pressure gradients. The governing equations for small amplitude transverse oscillations, $w(r^*, \varphi, t^*)$, of a flat, spinning, linearly elastic disk has been presented by several authors [2, 5, 9]. With the inclusion of the aerodynamic loading and acoustic excitation and the introduction of the dimensionless quantities

$$w = \frac{w^*}{h}, \quad r = \frac{r^*}{b}, \quad \kappa = \frac{a}{b}, \quad t = \frac{t^*}{t_0}, \quad \Omega = \Omega^* t_0, \quad \Delta p = \frac{\Delta p^* t_0^2}{\rho h^2}, \tag{1}$$

where t^* represents time and $t_0 = (12(1-\nu)\rho b^4/(Eh^2))^{1/2}$ is a characteristic time constant, the field equations become

$$w_{,tt} + 2\Omega w_{,t\varphi} + \Omega^2 w_{,\varphi\varphi} + D[w_{,t}] + K[w] = \Delta p + \frac{1}{r} f(t)\bigg|_A, \tag{2}$$

where $f(t)$ is the acoustic excitation and A is the surface of excitation. Further,

$$K[w] = \nabla^4 w - \frac{1}{r}(rN_{rr}w_{,r})_{,r} - \frac{1}{r^2}(N_{\varphi\varphi}w_{,\varphi\varphi}) \tag{3}$$

is the self-adjoint stiffness operator modelling the bending stiffness and stiffness caused by the membrane stresses $(N_{rr}, N_{\varphi\varphi})$ of rotation. Substrate material viscoelastic effects are introduced through the self-adjoint, positive definite operator $D[w_{,t}] = \nabla^4 w_{,t}$, where the material damping is assumed to be proportional to the rate of bending strain [2, 9]. Finally, the boundary and the periodicity conditions for the plate deflection and the aerodynamic pressure are given by

$$\begin{gathered} w|_{r=\kappa} = 0, \quad (w_{,rr} + \nu(w_{,\varphi\varphi} + w_{,r}))|_{r=1} = 0, \\ w_r|_{r=\kappa} = 0, \quad ((\nabla^2 w)_{,r} + (1-\nu)(w_{,r} - w)_{,\varphi\varphi})|_{r=1} = 0, \\ w(r, \varphi, t) = w(r, \varphi + 2\pi, t), \quad \Delta p(\kappa, \varphi, t) = 0, \quad \Delta p(1, \varphi, t) = 0. \end{gathered} \tag{4}$$

Note that there are other boundary conditions governing the in-plane displacements of the disk, which are taken into account in calculating the membrane stresses due to rotation [11].

2.1. AEROELASTIC COUPLING

The Reynolds number of the flow in a hard disk drive is greater than that encountered in a floppy disk drive. Accordingly, hydrodynamic lubrication theory, describing the pressure in a thin film between the disk and a rigid enclosure, is not directly applicable in this problem. At the same time, a model of the pressure loading based on the complete Navier–Stokes equation is highly complicated to provide analytical design tools. For this

reason, we desire a simple model of aerodynamic loading that retains some features of the lubrication model.

A main feature of this lubrication model is that Δp can be described in terms of a distributed viscous damping that rotates at half the rotation speed of the disk [2]. The rotating damping speed being half of the disk rotation speed arises because at very low Reynolds numbers, the mean flow speed in the gap is half of the disk speed. In our modelling, we retain the rotating damping model because it describes qualitatively many of the experimental observations. However, no prescription of the speed of the rotating damping is provided. Instead, the speed will be deduced experimentally. Further, in the lubrication model, the speed of rotating damping is independent of the mode of vibration of the disk. We now allow the rotating damping speed to depend on the number of nodal diameters of the excited mode. This allows the following generalization of the aerodynamic loading (in a ground-fixed frame):

$$\nabla^2(\Delta p) = -\alpha(w_{,t} + (\Omega - \Omega_{dmn})w_{,\varphi}). \tag{5}$$

where ∇^2 is the Laplacian operator, α is a positive parameter dependent on the viscosity of the fluid, the rotation speed Ω and the gap width. Further, (m, n) are the nodal circle and nodal diameter number of the particular mode of vibration respectively. Thus, this generalization allows the rotating damping speed to depend on the excited mode, as well as allowing a non-linear variation of the rotating damping speed with disk speed. Choosing the speed of rotating damping $\Omega_{dmn} = \Omega/2$ yields the lubrication theory model for pressure loading. Note also that we are neglecting the effects of radial flow [4] in this analysis because the radial flow effect in this shrouded disk is shown experimentally not to be significant. This is borne out by the experiments presented later in this paper. Lastly, to address a question: are outer disks in a disk stack more susceptible to flutter? The speed of rotating damping with respect to the disk is expected to be greater in the gap between the disk and rigid enclosure than between the two corotating disks since the mean flow in the disk-rigid enclosure gap is smaller because of the high transverse shear. For this reason the highest probability for flutter occurs in a single disk with a base plate and a rigid cover on each side. Based on this reasoning we focus on a single disk in the disk stack. The following subsections on the "coupled eigenvalue problem" and "extraction of model parameters" are based on Hansen *et al.* [9].

2.2. COUPLED EIGENVALUE PROBLEM

Noting that the Laplacian is a self-adjoint operator and considering the boundary conditions on Δp, the assumed aerodynamic loading (5) can be inverted with the help of Green functions [5], $\Delta p = -C[w_{,t} + (\Omega - \Omega_{dmn})w_{,\varphi}]$, with C being a self-adjoint operator. A solution of the separable form is assumed,

$$w(r, \varphi, t) = R_{mn}(r)\mathrm{e}^{\mathrm{i}n\varphi + \lambda t}, \tag{6}$$

where $R_{mn}(r)$ are in general normalized complex valued functions and (m, n) are the number of nodal circles and diameters, respectively, of the mode in question. Substituting this form into equation (2), in the absence of acoustic excitation, yields the coupled aeroelastic eigenvalue problem

$$(\lambda^2 + \mathrm{i}2\lambda n\Omega - n^2\lambda^2)R_{mn} + K_n^r[R_{mn}] + \lambda D_n^r[R_{mn}] + (\lambda + \mathrm{i}n(\Omega - \Omega_{dmn}))C_n^r[R_{mn}] = 0, \tag{7}$$

where (K_n^r, D_n^r, C_n^r) are one-dimensional differential operators obtained by the substitution of the assumed mode shape into the spatial operators (K, D, C). Aeroelastic coupling between the modes possessing different number of nodal circles is neglected [9]. Taking the inner products $\langle u(r), v(r)\rangle = \int_\kappa^1 u(r)\bar{v}(r)r\,\mathrm{d}r$, with the bar representing the complex conjugate, of equation (7) with each normalized eigenfunction gives

$$(\lambda_{mn} + \mathrm{i}n\Omega)^2 + \omega_{mn}^2 + c_{mn}(\lambda_{mn} + \mathrm{i}n(\Omega - \Omega'_{dmn})) = 0, \tag{8}$$

where $\omega_{mn}^2 = \langle R_{mn}, K_r^n[R_{mn}]\rangle$ are the uncoupled natural frequencies of the modes (corotating frame), and are given by [11] as

$$\omega_{mn}^2 \approx (\omega_{mn}^{st})^2 + s_{mn}\Omega^2, \tag{9}$$

where ω_{mn}^{st} is the natural frequency of the same mode in a stationary disk. Further

$$c_{mn} = \langle R_{mn}, D_r^n[R_m]\rangle + \langle R_{mn}, C_r^n[R_m]\rangle \tag{10}$$

represents the combined effects of structural and corotating fluid damping, and

$$\Omega'_{dmn} = \Omega_{dmn}\frac{\langle R_m, C_r^n[R_m]\rangle}{c_{mn}}, \tag{11}$$

where Ω'_{dmn} is the effective rotating damping speed modified by the ratio of aerodynamic corotating damping to the total corotating damping of the mode. Thus, the greater the structural dissipation of the substrate material, the lower the effective rotating damping speed. Solution for the eigenvalues under assumption of weak damping yields

$$\lambda_{mn}^F = -\frac{c_{mn}}{2}\left(1 + \frac{n\Omega'_{dmn}}{\omega_{mn}}\right) - \mathrm{i}(\omega_{mn} + n\Omega), \quad \lambda_{mn}^B = -\frac{c_{mn}}{2}\left(1 - \frac{n\Omega'_{dmn}}{\omega_{mn}}\right) + \mathrm{i}(\omega_{mn} - n\Omega), \tag{12}$$

where the superscripts F and B refer to forward or backward travelling waves that propagate in the direction of disk rotation or against it respectively. These waves are abbreviated FTW and BTW respectively. Thus, the immediate effect of the circulatory term in the aerodynamic pressure is to cause forward travelling waves to be more highly damped than the backward travelling waves. This phenomenon is seen in the hard disk drive at subcritical speeds (see section 1). Further, the damping of a backward travelling wave in equation (12) can vanish at the onset of aeroelastic flutter. The condition for the onset of aeroelastic travelling wave flutter is

$$\frac{\omega_{mn}}{n} = \Omega'_{dmn} \tag{13}$$

or when the effective rotating damping speed equals an uncoupled wave speed on the disk. Similarly, from equation (12), we see that the frequencies of the backward and forward travelling waves split and at a critical speed, $\Omega_c = \omega_{mn}/n$, the frequency of a BTW equals zero. Lastly, we note that the FRF of the disk, acoustically excited at $(r_f^*, 0)$ and measured at (r_x^*, φ_x), corresponding to the eigenvalue problem (8), is [12]

$$H(\omega) \approx R_{mn}(r_f^*)R_{mn}(r_x^*)(H_{mn}\mathrm{e}^{\mathrm{i}n\varphi_x} + \bar{H}_{mn}(-\omega)\mathrm{e}^{\mathrm{i}n\varphi_x}), \tag{14}$$

where

$$H_{mn}(\omega) = 1/[\omega_{mn}^2 - (\omega + n\Omega)^2 + \mathrm{i}c_{mn}(\omega + n\Omega - n\Omega'_{dmn})].$$

A detailed derivation of equation (14) is presented in Hansen *et al.* [9].

2.3. EXTRACTION OF MODELS PARAMETERS

From equations (9) and (12) we see that the model parameters that need to be identified from the experiment are (s_{mn}, c_{mn}, Ω'_{dmn}) for each mode at each disk rotation speed. These parameters represent, respectively, the stiffness coefficient due to rotation for the modal natural frequency, the total corotating modal damping, and the effective rotating damping speed in that mode. These parameters can be obtained from the FRF. Once the wave poles, ($\alpha^F_{mn} + i\omega^F_{mn}$, $\alpha^B_{mn} + i\omega^B_{mn}$), corresponding to the forward and backward travelling waves are identified in the FRF, equations (9) and (12) give

$$s_{mn} = \frac{[(\omega^F_{mn} + \omega^B_{mn}/2)^2 - (\omega^{st}_{mn})^2]}{\Omega^2},$$

$$c_{mn} = \alpha^F_{mn} + \alpha^B_{mn}, \quad c_{mn}\Omega'_{dmn} = \frac{\omega_{mn}}{n}(\alpha^F_{mn} - \alpha^B_{mn}). \tag{15}$$

The experimentally obtained damping factors of the wave poles in the FRF, (α^F_{mn}, α^B_{mn}) are usually small, and to avoid errors in calculating Ω'_{dmn} through division by c_{mn}, we will calculate directly c_{mn} and the product $c_{mn}\Omega'_{dmn}$ through the above relations.

3. EXPERIMENTAL ANALYSIS

Experiments were performed to estimate the flutter speed of a 3·5 in. hard disk drive. The flutter speed was estimated from condition (13) through the extrapolation of the effective rotating damping speeds and wave speeds. The effects of the air gap, and the distance between the disk surface and cover on the critical speeds and flutter speeds was also investigated by performing the test with the cover positioned at different gaps.

3.1. EXPERIMENTAL SET-UP

The out-of-plane vibration of the disk was measured using a laser Doppler displacement meter (LDDM) through a hole (1 mm in diameter) in the cover as shown in Figure 2. A speaker (0·1 W, 8 Ω, 2 in in diameter) was used to excite the disk through a hole (20 mm in

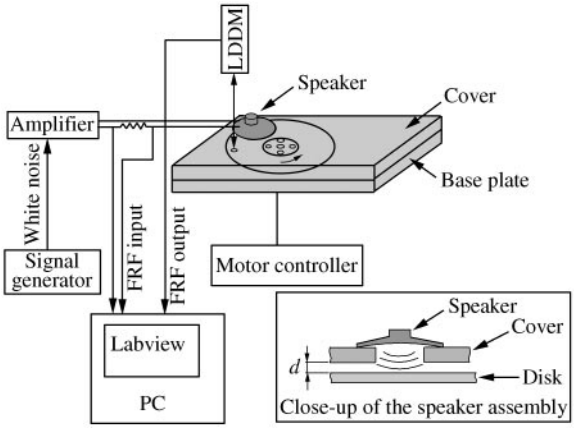

Figure 2. Experimental set-up for measuring the FRF of a disk.

diameter) in the cover. The current to the speaker gave a measure of the input to the frequency response function and the signal from the disk vibration was the output. A white-noise excitation signal was input to the speaker and the FRF was measured at the disk speeds from 6,000 to 19,800 rpm.

LABVIEW was used to collect the data and calculate the FRF from the input/output signals. The damping factors of each mode were calculated by curve fits in MATLAB to the measured FRF.

3.2. ESTIMATION OF WAVE FREQUENCIES AND DAMPING FACTORS

In this experiment, the frequency resolution was 0·183 Hz (6 kHz cut-off frequency and 65,536 frame size) and the 3 dB bandwidth of the resonance peaks was in the range of 0·5–5 Hz. With this frequency resolution, sufficient data were recorded for both the forward and backward resonance peaks to estimate the damping factors.

The FRF was processed on a PC to obtain the wave frequencies and damping factors of four modes ($m = 0$ and $n = 2, 3, 4, 5$). Because the (0, 1) mode has no critical speed, i.e., $\omega_{01} > \Omega$, $\forall\Omega$ [13], and assuming $\Omega_{d01} < \Omega$, it is expected that no flutter can occur in this mode. For this reason, the (0, 1) mode was not measured. To improve the estimation of modal parameters, a large number of averages were required (approximately 100). Because of the large frame size in the FRF, the higher-frequency resolution required extended recording time to collect the data with sufficient averaging. Fluctuation of the disk speed was found during the extended recording time. This rotation speed fluctuation can cause error in calculating the modal parameters. For example, a 0·5 Hz fluctuation in rotation speed during the measurement will cause approximately $\pm 0{\cdot}5 \times n$Hz difference in the forward and backward wave frequency peak for (0, n) mode. This speed fluctuation causes significant error in evaluating the damping factor. Because the typical 3 dB bandwidth of the backward resonance peaks in this experiment is in the range of 0·5–2 H, an error of $\pm$ 2·5 Hz (say, for (0, 5) mode) by speed fluctuation causes the evaluated damping factors to be much larger than the correct value. For this reason, a frequency response spectrum averaged over 100 ensembles causes significant error in the damping measurement. To minimize the error in the damping factors due to speed fluctuation, the FRF was averaged after only three ensembles and the speed fluctuation was monitored through the runout frequency of the disk vibration. For each such data set, the speed was constant. Thirty three such averaged data sets were collected (each from three averaged ensembles). The speed may vary from one data set to another. These speed fluctuations, Δf, were used to correct the resonance peaks for different data sets by shifting frequencies by $\pm n \times \Delta f$ Hz. The peaks in each data set were adjusted to coincide and an average FRF over 33 data sets was calculated and used to obtain the wave frequencies and damping factors.

The peak from each wave frequency was assumed to describe the single-degree-of-freedom (s.d.o.f.) the oscillator. The curve fitting was performed on the amplitude of the FRF near each peak to obtain the modal parameters. The wave frequencies and damping factors are calculated with different bandwidth taken near the peak in curve fitting. The curve fits were performed for 12 different bandwidths for the same peak. The modal parameters from the bandwidth that result in the largest correlation coefficient during curve fitting were chosen as the values of the wave frequency and damping factor.

The forward and backward wave frequencies were measured at disk speeds from 6,000 to 19,800 rpm. This experiment was repeated with changing air gaps between the disk and the cover, d. The natural frequencies at each speed from forward and backward wave frequencies are obtained using the relationships $\omega_{0n}^F = \omega_{0n} + n\Omega$, $\omega_{0n}^B \approx \omega_{0n} - n\Omega$ and are

curve fitted by equation (9), $\omega_{0n}^2 = \omega_{0n}^{st^2} + s_{0n}\Omega^2$. The results of the curve fits are shown in Table 1. The correlation coefficients R^2 in Table 1 show that equation (9) is a reasonable approximation of the relationship between the disk speed and the natural frequency for all the tests. The wave frequencies from experiments are shown in Figure 3. Also shown in Figure 3 are the wave frequencies after curve fitting based on relationship (9).

The estimated critical speeds with changing air gap are shown in Figure 4. It is observed that the critical speeds of the four modes are higher when the disk is uncovered. The

TABLE 1

Natural frequencies ω_{0n}^{st}, centrifugal stiffening coefficients s_{0n} and correlation coefficients of curve fits

	d (in)	$(0,2)B$	$(0,2)F$	$(0,3)B$	$(0,3)F$	$(0,4)B$	$(0,4)F$	$(0,5)B$	$(0,5)F$
ω_{0n}^{st}	0·05	719·58	708·47	1161·4	1154·3	1911·9	1904·0	2899·5	2891·4
	0·1	722·16	711·23	1164·4	1158·4	1916·1	1909·3	2904·9	2897·7
	0·15	721·21	712·13	1164·7	1160·3	1916·3	1911·1	2904·7	2899·6
	0·25	723·23	713·91	1166·1	1161·7	1917·7	1912·6	2906·5	2900·7
	0·35	724·70	715·01	1167·0	1162·8	1919·0	1914·2	2908·3	2903·2
	Open	724·38	715·47	1166·4	1162·7	1918·2	1913·9	2907·7	2903·0
s_{0n}	0·05	1·5434	1·4751	1·9984	1·8822	2·4164	2·2718	2·7831	2·5803
	0·1	1·5416	1·5001	1·9844	1·9053	2·4029	2·2997	2·7775	2·6345
	0·15	1·5525	1·5096	1·9955	1·9174	2·4205	2·3191	2·8070	2·6596
	0·25	1·5428	1·5083	1·9846	1·9151	2·4070	2·3143	2·7826	2·6565
	0·35	1·5399	1·5066	1·9852	1·9187	2·4103	2·3198	2·7975	2·6678
	Open	1·5810	1·5470	2·0670	2·0020	2·5565	2·4657	3·0314	2·9045
R^2	0·05	0·99996	0·99998	0·99995	0·99997	0·99998	0·99998	0·99998	0·99998
	0·1	0·99998	0·99999	0·99998	0·99998	0·99998	0·99999	0·99999	0·99999
	0·15	0·99986	0·99999	0·99998	0·99999	0·99999	0·99999	0·99999	0·99999
	0·25	0·99998	0·99999	0·99997	0·99999	0·99998	0·99999	0·99999	0·99999
	0·35	0·99997	0·99999	0·99997	0·99998	0·99998	0·99999	0·99999	0·99999
	Open	0·99998	0·99999	0·99998	0·99999	0·99999	0·99999	0·99999	0·99999

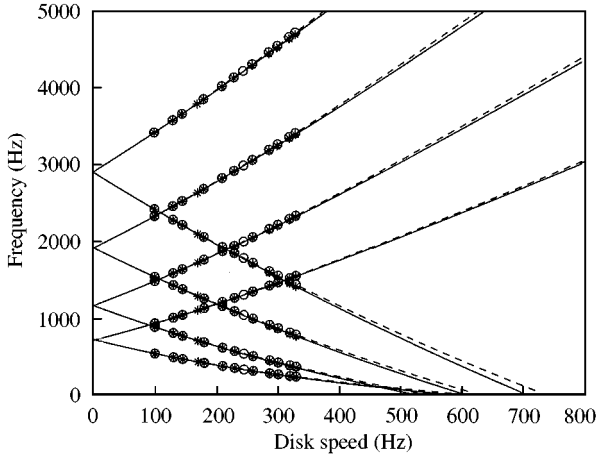

Figure 3. Wave frequencies: (∗), from measurement, and (——), from corresponding curve fit on ω_{0n} for the covered drive ($d = 0{\cdot}35$ in); (○), from measurement, and (- - - - -), from curve fit on ω_{0n} for the uncovered drive.

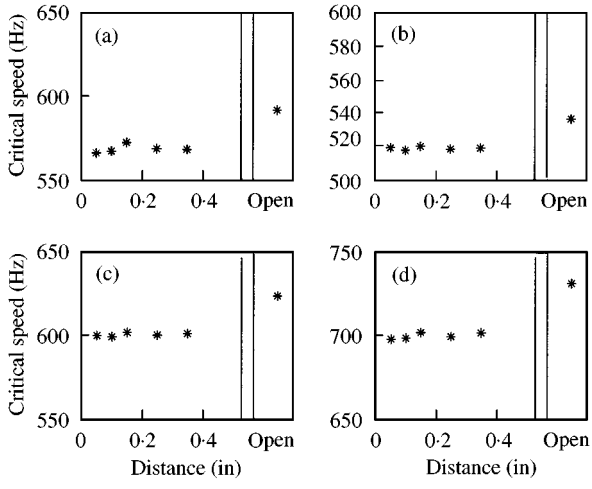

Figure 4. Critical speed versus air gap d: (a) (0, 2) mode; (b) (0, 34 mode; (c) (0, 4) mode; (d) (0, 5) mode.

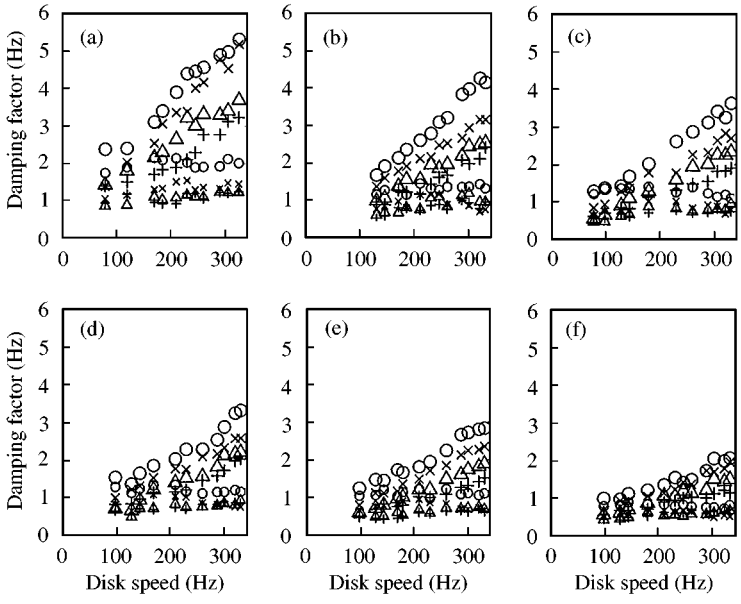

Figure 5. Damping factors versus disk speed: (a) $d = 0{\cdot}05$; (b) $d = 0{\cdot}1$; (c) $d = 0{\cdot}15$; (d) $d = 0{\cdot}25$; (e) $d = 0{\cdot}35$ in; (f) uncovered, (○), (0, 2) mode; (×) (0, 3) mode; (△) (0, 4) mode; (+) (0, 5) mode (large marker, FTW; small marker, BTW).

percentage increases in critical speeds of the uncovered case, compared to the averaged critical speeds for covered cases, are 4·1, 3·4, 3·9, 4·5% for the 2, 3, 4, 5 modes respectively.

The estimated damping factors of the forward/backward travelling waves for the four modes at different gap width, as function of disk speed, are shown in Figure 5. It is observed that the damping factors of FTWs are substantially larger than those of the BTWs. The differences increase with the increasing disk speed. We also see in Figure 6 that the absolute values of damping factors of the FTWs and BTWs tend to decrease with increasing air gap.

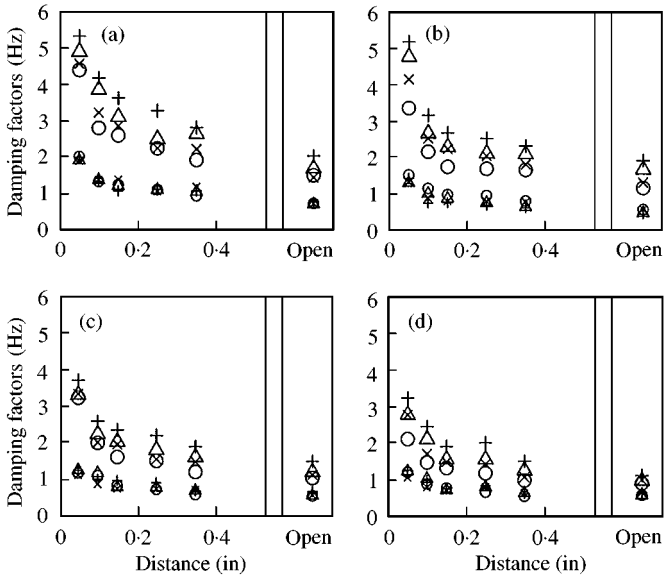

Figure 6. Damping factors versus air gap d: (a) (0, 2) mode; (b) (0, 3) mode; (c) (0, 4) mode; (d) (0, 5) mode. (○) 13,800 rpm; (×) 15,600 rpm; (△) 17,400 rpm; (+), 19,800 rpm (large marker, FTW; small marker, BTW).

3.3. ESTIMATION OF AEROELASTIC PARAMETERS AND FLUTTER SPEED IN DISK DRIVE

After the damping factors α_{0n}^F and α_{0n}^B are obtained, the two aeroelastic parameters c_{0n} and $c_{0n}\Omega'_{d0n}$ can be extracted as shown in equation (15)

$$c_{0n} \approx \alpha_{0n}^F + \alpha_{0n}^B, \quad c_{0n}\Omega'_{d0n} = \omega_{0n}\frac{(\alpha_{0n}^F - \alpha_{0n}^B)}{n}.$$

The damping coefficients c_{0n} tend to increase linearly with disk speed, whereas the product $c_{0n}\Omega'_{d0n}$ tends to increase non-linearly with disk speed. The linear and second order polynomial functions of the disk speed were chosen to curve fit the two aeroelastic parameters c_{0n} and $c_{0n}\Omega'_{d0n}$, respectively,

$$c_{0n} \approx c_1 + c_2\Omega, \quad c_{0n}\Omega'_{d0n} \approx c_3\Omega + c_4\Omega^2. \tag{16}$$

Typical values of c_{0n} and $c_{0n}\Omega'_{d0n}$ of the four modes with the increasing disk speed and their curve fits based on equations (16) are shown in Figure 7 ($d = 0{\cdot}15$ in). The four fitting coefficients c_1, c_2, c_3, c_4 and the correlation coefficients R^2 for the four modes are shown in Table 2.

With these expressions for c_{0n} and $c_{0n}\Omega'_{d0n}$ the effective damping speed Ω'_{d0n} can be estimated as

$$\Omega'_{d0n} \approx \frac{c_3\Omega + c_4\Omega^2}{c_1 + c_2\Omega}. \tag{17}$$

By extrapolating the curves for the effective damping speed, the flutter speed of each case tested here can be estimated by the intersection of the wave speed curve ω_{0n}/n and the effective damping speed curve Ω'_{d0n} of each mode. The effective damping speed estimated in this manner together with wave speed for each mode and air gap are shown in Figure 8.

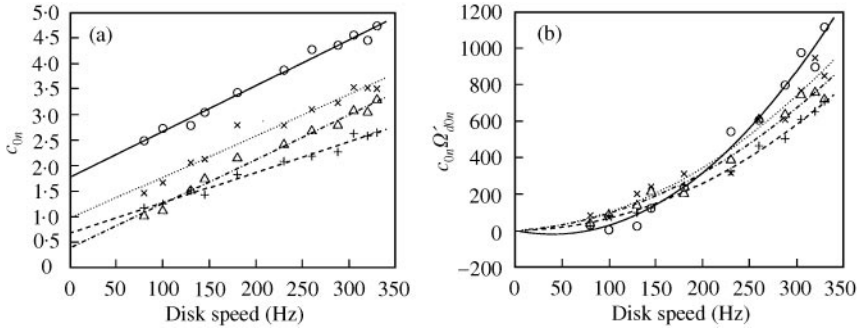

Figure 7. Aeroelastic parameters (a) c_{0n} and (b) $c_{0n}\Omega'_{d0n}$ and their curve fits: (○), mode; (×) (0, 3) mode, (△), (0, 4) mode; (+) (0, 5) mode.

TABLE 2

Curve fit coefficients to c_{0n} and $c_{0n}\Omega'_{d0n}$ and their correlation coefficients

Mode	d (in)	c_1	$c_2 \times 100$	R^2 (c_{0n})	c_3	$c_4 \times 100$	R^2 $(c_{0n}\Omega'_{d0n})$
(0, 2)	0·05	2·9522	1·3799	0·97695	1·0893	1·0676	0·95266
	0·1	1·0753	1·4102	0·98259	−0·1260	1·2273	0·98578
	0·15	1·7703	0·8978	0·98582	−1·0339	1·3136	0·98184
	0·25	1·7014	0·7632	0·89043	−0·5847	1·0146	0·97915
	0·35	1·4710	0·7498	0·96845	−0·1855	0·79367	0·96430
	Open	1·1776	0·4731	0·92048	−0·3222	0·63575	0·95530
(0, 3)	0·05	1·1601	1·6783	0·99000	1·26250	1·17030	0·96069
	0·1	1·3046	0·8527	0·93587	0·40608	0·84232	0·94322
	0·15	0·9622	0·8110	0·96367	0·27104	0·73037	0·95423
	0·25	1·1576	0·6635	0·93922	0·00745	0·73655	0·96577
	0·35	0·9253	0·6602	0·97175	−0·4134	0·83367	0·97644
	Open	0·7348	0·4969	0·95462	−0·1303	0·60916	0·96551
(0, 4)	0·05	1·4375	1·0963	0·96456	3·4340	0·14476	0·93886
	0·1	0·4031	1·0163	0·93717	0·89724	0·44442	0·92928
	0·15	0·3813	0·8705	0·98368	0·28137	0·64845	0·96922
	0·25	0·3729	0·8034	0·94507	−0·1344	0·70821	0·96945
	0·35	0·3272	0·6872	0·98362	0·20321	0·50276	0·98952
	Open	0·4050	0·5183	0·96570	0·35333	0·31367	0·91999
(0, 5)	0·05	1·3301	0·9142	0·89593	1·16730	0·78628	0·91255
	0·1	0·3695	0·8762	0·92372	0·08672	0·74092	0·94534
	0·15	0·6704	0·6003	0·98087	0·04142	0·63089	0·99232
	0·25	0·5874	0·6482	0·94424	0·25690	0·52775	0·94665
	0·35	0·4117	0·5111	0·97414	0·50409	0·29189	0·89809
	Open	0·5737	0·3843	0·95549	0·65017	0·08712	0·89376

The trend of effective damping speed in each mode with varying air gap can be observed in this plot. For example, in the (0, 4) mode there exists no flutter speed when the air gap is 0·05 in. As the air gap increases, the effective damping speed intersects the wave speed curve when the air gap lies between 0·1 and 0·15 in. As the air gap increases further, the slope of the effective damping speed curve decreases and the intersection with the wave speed vanishes for $0{\cdot}35 < d < \infty$. Even though this behavior for other modes is not as clear as for

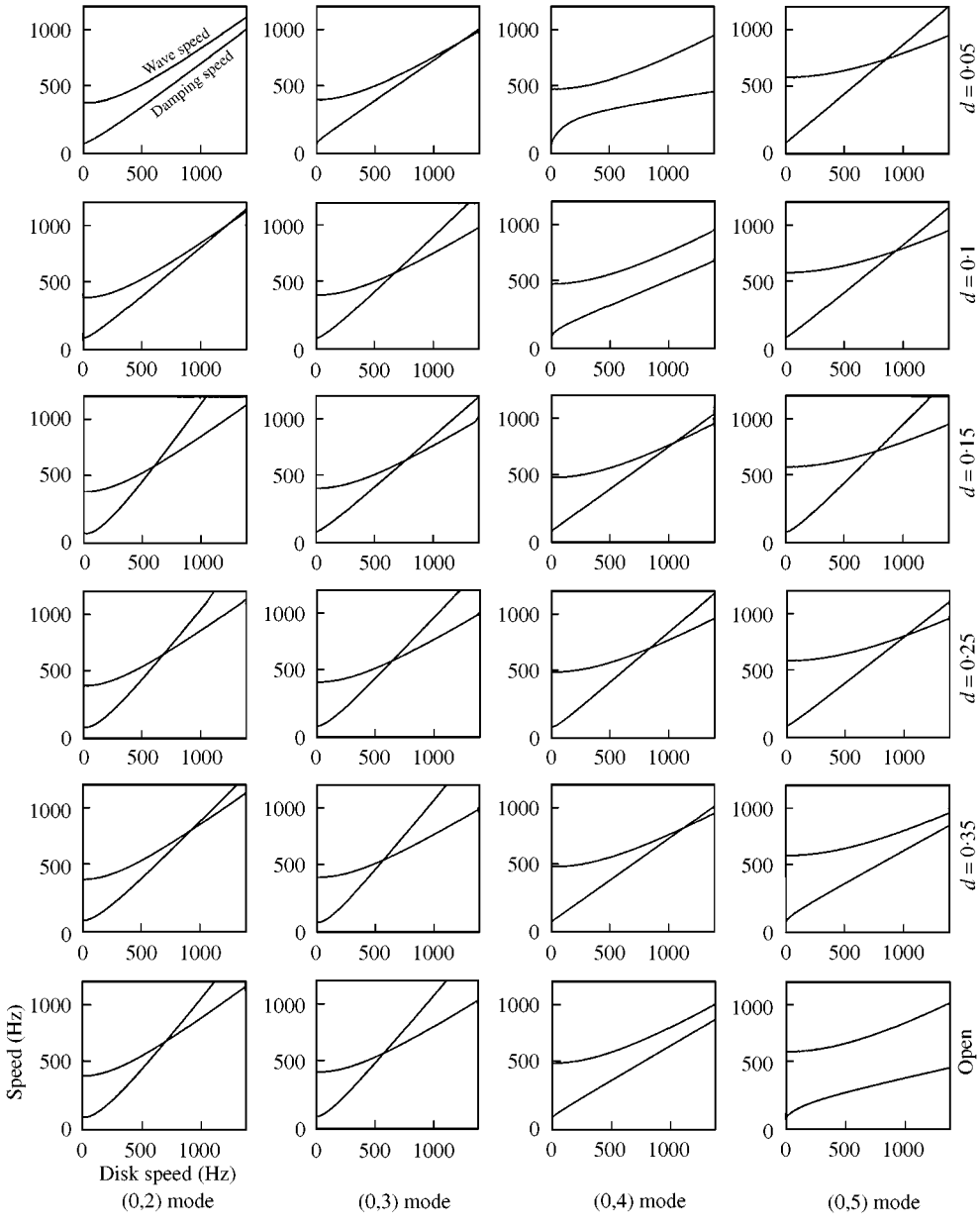

Figure 8. Wave speeds ω_{0n}/n and damping speeds Ω'_{d0n} for each mode under air gap change.

the (0, 4) mode in Figure 8, the general trend can be seen in Figure 9. For the (0, 2) and (0, 3) modes, the flutter speed decreases with increasing air gap, whereas for the (0, 5) mode the flutter speed increases with the increasing air gap. The flutter speed for each mode and each air gap is listed in Table 3.

The aeroelastic flutter is predicted to occur in the (0, 3) mode at each air gap except $d = 0{\cdot}15$ in. The smallest flutter speed was predicted to be 34 970 rpm ($d = 0{\cdot}35$ in, (0, 3) mode).

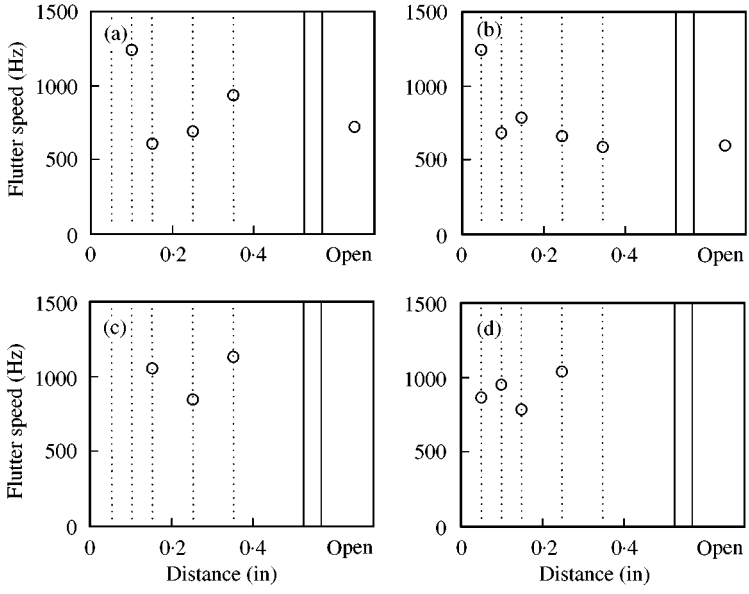

Figure 9. Flutter speed of each mode versus air gap: (a) (0, 2) mode; (b) (0, 3) mode; (c) (0, 4) mode; (d) (0, 5) mode.

TABLE 3

Flutter speeds (rpm) in the four modes under the change of air gap

d (in)	(0, 2) mode	(0, 3) mode	(0, 4) mode	(0, 5) mode
0·05	None	74,418	None	51,451
0·1	74,592	40,738	None	56,600
0·15	36,693	46,931	63,420	46,567
0·25	39,780	39,404	50,853	61,770
0·35	41,585	34,970	67,950	None
Open	43,195	35,420	None	None

4. DISCUSSION

The natural frequencies and critical speeds of (0, 2) (0, 3), (0, 4) and (0, 5) modes were found to be consistently greater for an uncovered disk (see Figures 2 and 3). The removal of the cover decreases the bending stiffness of the spindle. Because only (0, 1) mode on the disk is coupled to spindle bending [14] it is expected that the removal of the cover decreases the frequency of (0, 1) mode while maintaining an unchanged frequencies of the higher modes. For this reason, the observed increase in the frequencies of the higher modes for the uncovered disk were unexpected. One possible reason for this phenomenon is based on the presence of thermal gradients on the rotating disk. Due to friction, heat is generated in the bearings and transferred through the collars to the disk. The resulting temperature gradients modify the membrane stresses and thus the frequencies of the rotating disk. Owing to flow re-circulation in a covered disk, the temperature of the airflow is significantly greater than in an uncovered case. Consequently, the radial temperature gradient of the uncovered disk is expected to be larger than in the covered disk. This can result in higher natural frequencies in the uncovered case compared to the covered case. This agrees with

the results of Nieh and Mote [15], who found the increased critical speeds (for the (0, 2) and (0, 4) modes, numerically and experimentally) when bearing heating was applied at the inner radius of the rotating disk.

The decreasing air gap between the disk and the cover leads to increased damping factors (see Figure 6). Recently, Ono *et al.* [16] studied the effect of a partial squeeze air bearing plate, which is located on the top of the disk, on the amplitude of disk vibration. They found that the amplitude of the travelling wave of the lowest frequency decreases with the decreasing air gap between the disk surface and the air bearing plate at 7200 and 9600 rpm. The present paper supports and explains their observation.

Increased material damping in the disk substrate suppresses the onset of flutter. The increased modal damping of the substrate $\langle W_{0n}, D[W_{0n}]\rangle$, results in a decreased effective damping speed (equations (10) and (11)), and consequently a greater aeroelastic flutter speed. For a disk of given clamping ratio and a bending stiffness, it may be possible to choose a substrate material with sufficient internal damping to eliminate aeroelastic instability.

The damping factors predicted from the hydrodynamic lubrication theory correlate poorly with experimental results. A lower bound for the speed of aeroelastic flutter in this case is provided by the condition that the rotating damping speed $\Omega_d = \Omega/2$ equals the undamped wave speed ω_{0n}/n as the disk speed is increased. The inclusion of material damping through the effective rotating damping speed will increase this estimate. However, it is found in the experiments that there is no intersection of the rotating damping and wave curves as speed changed. This implies that use of hydrodynamic lubrication theory will never predict the flutter of the disk at any speed. The hydrodynamic lubrication theory for Δp [2, 5, 17] prescribes that c_{0n} and $c_{0n}\Omega'_{d0n}$ should be, respectively, constant and a linear function of the disk speed:

$$c_{0n} \approx c_5, \quad c_{0n}\Omega'_{d0n} \approx c_6\,\Omega. \tag{18}$$

R^2 for c_{0n} is zero by the definition of the correlation coefficient. The correlation coefficient for $c_{0n}\Omega'_{d0n}$ based on the curve fits (16) and (18) are shown in Figure 10. It can be seen that the R^2 values from the curve fit (16) lie within 0·9–1, whereas those from the curve fit (18) lie

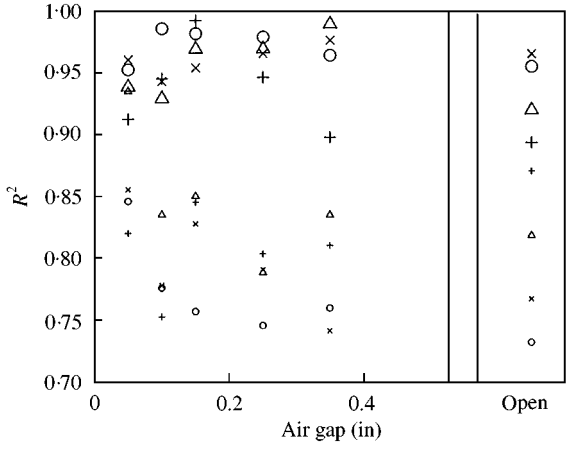

Figure 10. Correlation coefficients for $c_{0n}\Omega'_{d0n}$ based on the curve fits: (○) (0, 2) mode; (×) (0, 3) mode; (△) (0, 4) mode; (+) (0, 5) mode. Large markers, curve fit based on this work (equation (16)); small markers, curve fit based on lubrication theory (equation (18)).

in the range 0·75–0·85. From this, it can be said that hydrodynamic lubrication models of the airflow between a disk and the cover predict poorly the differential damping of the forward and backward travelling waves observed in the experiment.

The experiments indicate that the radial flow in the air gap does not significantly effect the aeroelastic flutter of the covered disk. Huang and Mote [3] note that secondary radial flow introduces a non-symmetric film stiffness acting on the spinning disk. This effect introduces an instability in addition to the rotating damping instability described in this work. Huang and Mote [3] show that at pre-flutter speeds, the effect of the film stiffness is to split the wave speeds of a given mode. In the present work, wave speeds calculated for a particular mode from the forward and backward travelling frequencies in the experiment, were found to be less than 2·5% apart from each other. This indicates that the effects of radial flow are not significant in the present disk drive. One reason for this could be that because of the radial shroud, the radial flow velocities are lower in a disk drive than in the open disk case considered by Huang and Mote [3].

Lastly, owing to the high Reynolds number in the gap of an actual disk drive the resulting flow is usually unsteady. The unsteadiness in the pressure fluctuations causes wide band excitation of the disk at all rotation speeds. The aeroelastic instability referred in this work, arises due to bulk or average motion of the fluid in the gap with respect to the disk and cannot predict the effects of turbulent pressure fluctuations on disk vibration at pre-flutter speeds. For this reason, aeroelastic travelling wave flutter can be regarded as an upper bound for the operation speeds in disk drives. The turbulence-induced vibration of disks can prevent the operation of disk drives even at pre-flutter speed.

5. CONCLUSIONS

An experimental technique is presented to estimate the flutter speed of a hard disk drive. Model parameters are extracted from the FRF of an acoustically excited disk spinning at a sub-critical speed ranging from 6,000 to 19,800 rpm. The flutter speed was estimated through the extrapolation of the effective rotating damping speed and wave speed. The results indicate that the aeroelastic flutter speed can be as low as 35,000 rpm and depend significantly on the air gap between the disk and the cover. The aeroelastic flutter instability is not predicted to occur near 20,000 rpm for the impending generation of the disk drives. However, if the substrate material remains unchanged, it is expected to be a problem for 30,000 + rpm drives. The technique presented in this paper can also be extended to estimate the flutter speed in optical disks including DVD and CDROM drives, which are already operating at supercritical speed and closer to their limits of aeroelastic instability. An experimental estimation of flutter speed in these devices will be important for the design of the impending generation of optical drives.

REFERENCES

1. S. CHONAN, Z. W. JIANG and Y. J. SHYU 1992 *Journal of Vibration and Acoustics* **114**, 283–286. Stability analysis of a 2″ floppy disk drive system and the optimum design of the disk stabilizer.
2. H. HOSAKA and S. CRANDALL 1992 *Acta Mechanica* **3**, 115–127. Self-excited vibrations of a flexible disk rotating on an air film above a flat surface.
3. F. HUANG and C. D. MOTE, JR. 1995 *Journal of Applied Mechanics* **62**, 764–771. On the instability mechanism of a disk rotating close to a rigid surface.
4. F. HUANG and C. D. MOTE, JR 1996 *Journal of Vibration and Acoustics* **118**, 657–662. Mathematical analysis of stability of a spinning disk under rotating, arbitrarily large damping forces.

5. A. A. RENSHAW 1998 *Journal of Applied Mechanics* **65**, 116–120. Critical speeds for floppy disks.
6. C. D'ANGELO and C. D. MOTE, JR 1993 *Journal of Sound and Vibration* **168**, 15–30. Aerodynamically excited vibration and flutter of a thin disk rotating at supercritical speed.
7. A. A. RENSHAW, C. D'ANGELO and C. D. MOTE, JR 1994 *Journal of Sound and Vibration* **177**, 577–590. Aerodynamically excited vibration of a rotating disk.
8. K. YASUDA, T. TORII and T. SHIMIZU 1992 *JSME International Journal* **35**, 347–352. Self excited oscillations of a circular disk rotating in air.
9. M. H. HANSEN, A. RAMAN and C. D. MOTE, JR 1999 *Danish center for applied mathematics and mechanics, Technical University of Denmark Technical Report No.* 605. Estimation of non-conservative aerodynamic pressure leading to flutter of spinning disks.
10. S. Y. LEE and S. K. KIM 1998 *Proceedings of the 9th International Symposium on Information Storage and Processing Systems*, Vol. 4, 81–90. Trends and mechanical issues in optical disk drives.
11. C. D'ANGELO and C. D. MOTE JR 1993 *Journal of Sound and Vibration* **168**, 1–14. Natural frequencies of a thin disk, clamped by thick collars with friction at the contacting surfaces, spinning at high rotation speed.
12. C.-W. LEE and M.-E. KIM 1995 *Journal of Sound and Vibration* **187**, 851–864. Separation and identification of travelling wave modes in rotating disk via directional spectral analysis.
13. A. A. RENSHAW and C. D. MOTE, JR 1992 *Journal of Applied Mechanics* **59**, 687–688. Absence of one nodal diameter critical speed modes in an axisymmetric rotating disk.
14. R. PARKER and C. D. MOTE JR 1996 *Journal of Applied Mechanics* **63**, 953–961. Vibration and coupling phenomena in asymmetric disk-spindle systems.
15. L. NIEH 1972 *Ph.D. Thesis, University of California, Berkeley*. Rotating disk stability. Spectral analysis and thermal effects.
16. K. ONO, E. MAEDA and H. YAMAURA 1999 *10th Annual Symposium on Information Storage and Processing Systems, Program and Extended Abstracts*. Suppression of disk flutter by squeeze air bearing plate.
17. I. PELECH and A. H. SHAPIRO 1964 *Journal of Applied Mechanics* **31**, 577–584. Flexible disk rotating on a gas film next to a wall.